ANALYSIS OF A STRINGER RUN-OUT CONCEPT INCLUDING DAMAGE INITIATION AND EVOLUTION AT THE INTERFACES

A. Blázquez*[1], J. Reinoso[1], F. París[1], A. Estefani[1], E. Arévalo[2], F. Cruz[3]

[1]*Group of Elasticity and Strength of Materials, School of Engineering, University of Seville, Camino de los Descubrimienos s/n, 41092 Seville, Spain*
[2]*Airbus ESIRSM R&T Structure Fuselage. Airbus Spain*
[3]*Airbus ESIRM/ESDR R&T Structure. Airbus Spain*
* *Corresponding Author: abg@esi.us.es*

Keywords: Interface Damage Mechanics, Composite-Stiffened Panels, FEM, Experimental Mechanics

Abstract

An experimental test was specifically designed in order to analyse the effect of the run-out of a stringer in a composite specimen. The test was carried out in several stages until the specimen collapse. The damaged regions and their geometric dimensions were identified by ultrasound inspections at the end of each stage. Several FEAs of the component were performed using the commercial software ABAQUS using two global-local approaches. The analysis of the results of the global model allows the geometric dimensions of the local one to be defined. Damage process will be included in the adhesive layer at this level. Finally, a correlation between the numerical predictions and the experimental results was accomplished.

1. Introduction

Composite stiffened panels are used in a wide range of application, especially in aircraft structures (for example fuselages and wings), due to their high strength/weight and stiffness/weight ratios. The variation in the transverse area of an aircraft wing or fuselage causes modifications in the number of stringers along the longitudinal direction. This originates the abruptly interruption of the load path, involving high stress concentrations that may lead to the development of damage. Indeed, the importance of these regions was shown to be critical in certain applications ([1, 2]), requiring to be studied in greater depth ([3, 4, 5]).

In this work a summary of the numerical and experimental studies of the run-out effect in a specifically designed specimen is presented. A detailed analysis of this problem has been recently published in [6]. This work is focused on the numerical simulation of the experimental test, including the onset of the damage and its progress at the nearly stages of the process. For this purpose, two global-local numerical approaches have been used, where the material nonlinearities related to the damage process are only considered at the local level. The commercial

Finite Element software ABAQUS has been used for this task. This software offers two different techniques to deal with global-local analysis: Submodeling and Shell-to-Solid Coupling.

2. Description of the experimetal test

The specimen considered in this work is shown in Figure 1. It is composed of a flat panel (skin) 300 mm in width at the central zone (increased to 500 mm at the load introduction area) and a stringer with Ω shape transverse section. Stringer and skin are made of IMA/M21E, a carbon-fiber composite material, they are co-bonded each other including a thin adhesive layer of polymeric resin EA9695.05K. The specimen also include a dummy frame made of the Al2024 T42 aluminum alloy, and a steel plate before this dummy frame (zones: Skin (2), Transition zone (2) and Reinforcement (2) in Figure 1) in order to avoid failures at this area.

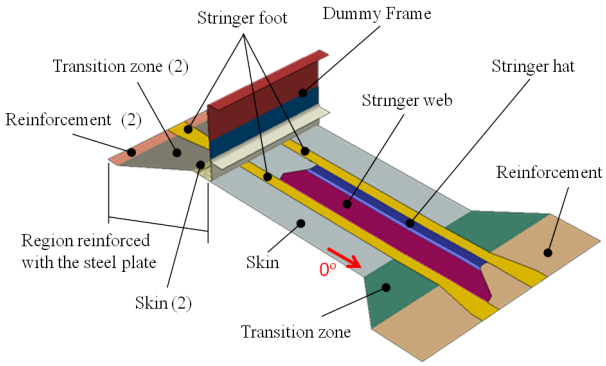

Figure 1. Solid modeling of the complete component

Stacking sequences corresponding to each zone of the skin and stringer are given in Table 1, including their resulting total thickness. Note that there is a transition zone between the central and the load introduction zone at both longitudinal extremes. The material orientation considered is also shown in Figure 1, indentifying the zero–degree reference direction.

Zone	Laminate	Total thickness
Ω Stringer	$[45/-45/0/0/0/90/0/0]_S$	2.944 mm
Skin	$[45/-45/90/0/-45/45/90/90]_\$$	2.760 mm
Skin (2)	Steel + Skin	6.760 mm
Transition	$[45/-45/90/0/0/-45/45/90/0/-45/45/90]_\$$	4.232 mm
Transition (2)	Steel + Transition	8.232 mm
Reinforcement	$[45/-45/0/90/0/-45/45/90/0/-45/45/90/0/-45/45/90]_\$$	5.704 mm
Reinforcement (2)	Steel + Reinforcement	9.704 mm

Table 1. Lay-ups of each zone of the specimen. The subscript $ denotes symmetry except for the last layer, which is the central layer of the total laminate

Regarding the experimental supporting conditions, both longitudinal extremes of the specimen were attached using an equally arranged series of rivets (Reinforcement and Reinforcement (2) in Figure 1). Additionally, at the borders of the central region of the specimen, a pair of lateral guides was placed restricting the displacement normal to the skin. They aim to simulate the

effect of additional stringers. Finally, the top flange of the dummy frame was attached to an auxiliary system which restricted normal displacements at the top flange and at the extreme, [6]. A universal traction machine, INSTRON 8806, was employed to run the test.

This specimen was tested until collapse. The test was interrupted at several stages in order to inspect the specimen visually and through ultrasound devices, specifically when noise occurred, allowing the damaged regions to be characterized. During the test procedure, the first audible sound was identified at 80 kN. Nevertheless, an inspection by ultrasound devices did not identify any evidence of damage. Thus, noise could be produced by fiber breakages and/or delaminations, that could not be detected with the used techniques. Continuing testing on the component, louder noises occurred at a load of 100 kN. The test was again interrupted and an

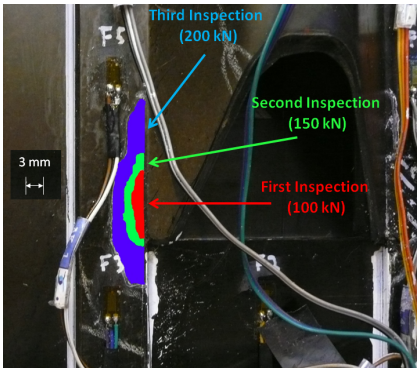

Figure 2. Damage evolution path at the stringer run-out region in the skin-stringer joint

additional inspection by ultrasound technique was performed. At this load level, two debondings at the skin-stringer interface became detectable at both sides of the specimen at the run-out regions. The geometric dimensions of the damaged regions registered (in red in Figure 2) were approximately between 3 and 4 mm in width and 7 and 8 mm in length. The subsequent inspection was carried out at 150 kN (in green in Figure 2), at which the debonding area had an approximate size of between 5 and 6 mm in width and between 12 and 15 mm in length. A final ultrasound inspection was carried out at 200 kN, identifying a damaged area (in blue in Figure 2) between 8 and 9 mm in width and between 50 and 55 mm in length. The structural collapse occurred at 430 kN. It was caused by the generalized failure of the skin-stringer interface and at the rivet rows located under the dummy frame.

3. Global Finite Element Analysis

3.1. Global Model Definition

Stringer, skin and dummy frame were modeled independently using the S4R ABAQUS shell elements. This is a 4-node first order (linear) element of reduced integration scheme with hourglassing control for finite strain applications. The adhesive layer was modeled employing C3D8R solid element. This element typology consists of an 8-node reduced integration linear element with hourglassing control for finite strain applications. Only one element is used through the thickness. This strategy allows the peel and transverse shear stress components (that affect the debonding phenomenon [3, 4]) to be computed.

Nodes of the shell elements belonging to the stringer and to the skin were offset towards the interfaces, Figure 3, in order to avoid the material overlapping between the adhesive layer and these entities. Thus, the nodal degrees of freedom between adjacent parts (skin-adhesive layer and stringer-adhesive layer pairs) were related by means of the `*TIE` ABAQUS constraint, [7].

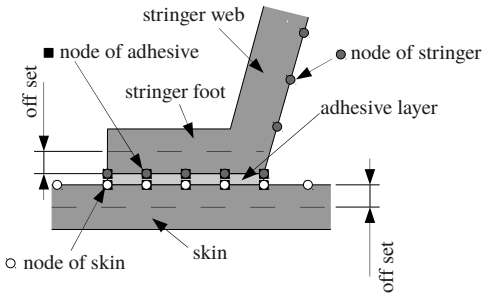

Figure 3. Graphical scheme of the co-bonded skin-stringer joint modeling procedure

The characteristic size for the shell elements was 3×3 mm^2. In the case of solid elements, as conforming meshes were considered, the previous value must be multiplied by the adhesive layer thickness (0.2 mm) to obtain the volume of the element, giving $3 \times 3 \times 0.2$ mm^3.

Support conditions on the dummy frame were modeled by avoiding the corresponding normal displacement components at its top flange and at its extreme transverse sections. Lateral guides were simulated by restricting the normal displacement along two lines near the border of the specimen. Mobile and fixed grips were modeled by means of two multipoint constraints (MPC), relating the displacements of some nodes to the displacement of a master node, in a way that the set of the nodes behaves as a rigid system. Therefore the load was applied at the master node on the mobile grip.

Due to the fact that the loading velocity was sufficiently low, a static numerical analysis was carried out, geometric nonlinear effects being included.

3.2. Global Model Results

Numerical stress distribution patterns at the run-out regions evolved continuously during the whole loading procedure without notable variations. Figure 4 shows peel and shear stress components at the adhesive layer for a load of 300 kN.

From the point of view of our proposed global-local analysis, two main general results can be obtained from Figure 4. First, as was expected, the most critical area in the specimen was the run-out region. And second, these stress fields were used in order to make a decision with regard to the most suitable characteristic sizes for subsequent local models. In this way, a zone approximately 90 mm in length around the run-out region was selected for the local analysis. This size was slightly increased in order to have a transition zone for the regularization of the boundary conditions transfered from the global model. Figure 5 shows schematically the location and size of the local model to be managed.

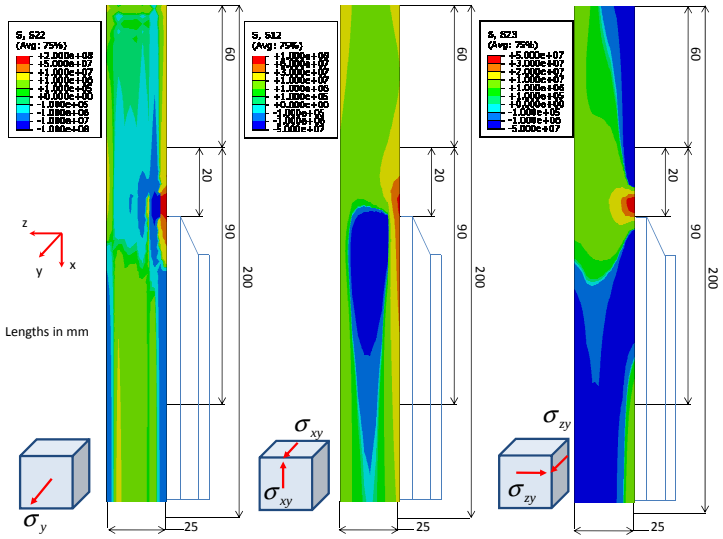

Figure 4. Stress distribution at the adhesive layer near the stringer run-out region at a load level of 300 kN

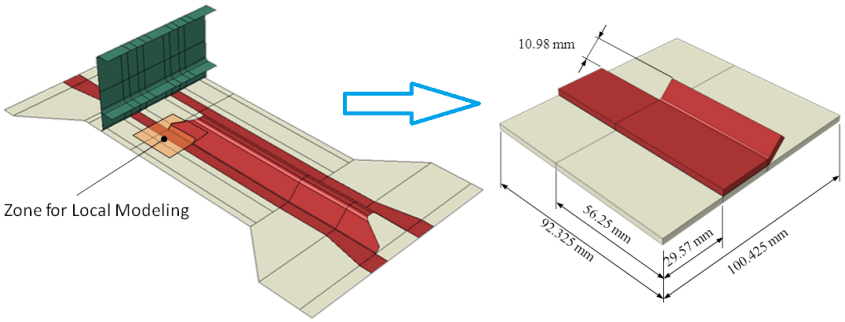

Figure 5. Zone selected for local analysis

4. Local Finite Element Analysis

ABAQUS offers two techniques for performing the local analysis: Submodeling and Shell-to-Solid Coupling.

- The Submodeling technique solves the global and the local models independently (in different computations). First, the full global model (without any specific mesh refinement in the zone of interest) is solved for the full load step (which can be divided in any number of substeps). Subsequently, a separated local model is solved using the results of the global one as boundary conditions on the surfaces that delimit the local model. Therefore, the local model evolution does not have any influence on the global one.

- The Shell-to-Solid Coupling technique only requires one computation in which the local model (with a refined mesh) is inserted into the global one (with a coarse mesh). Both meshes are coupled numerically. In this way, any mechanical feature included at the local level will affect the response of the complete model.

Regarding the resulting mesh characteristics of the local models, the C3D20R ABAQUS element was selected to mesh the corresponding portions of the skin and the stringer. This is a second order (parabolic) reduced integration element with 20 nodes that can include several layers to model composites. Damage along the interface has been considered using the cohesive zone model, [8], where the COH3D8 element implemented in ABAQUS was employed. This is a linear element with 8 nodes. A cohesive model with a Linear Traction-Separation Law, with a thickness of 0.2 mm and a with decoupled stiffness matrix was selected, [7]. The mechanical characteristics of the adhesive layer were: E_N = 1476.8 Mpa, G_T = 568 Mpa, σ_{Ic} = 25.1 Mpa, $\tau_{IIc} = \tau_{IIIc}$ = 50 Mpa, G_{IC} = 300 J/m^2 and $G_{IIC} = G_{IIIC}$ = 800 J/m^2. The maximum normal stress was considered as damage onset criterion, whereas the Benzeggagh and Keane Fracture Criterion ([9]), extended to three dimensional cases, was selected for the mixing failure.

Figure 6 shows a detail of the resulting mesh used at the local level, 4×4 cohesive elements of the adhesive layer correspond to 1 solid element of the skin or the stringer. Thus, the non-conforming character between the meshes arise from the number and from the integration order of the elements involved. In [6] all these features are analysed.

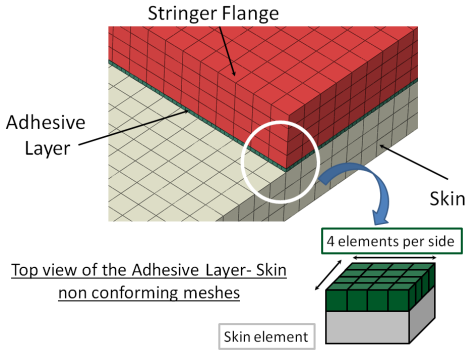

Figure 6. Nonconforming FE approach concerning nodal locations for Models 2 and 3

4.1. Local level results

Due to the fact that the damage process is included only at the local level, in order to obtain satisfactory results using the Submodeling technique the damage has to be small enough that the global response of the component were not affected by the damage onset and evolution. In order to determine this limit load, in [6] the solution of the local model with consideration of the damage along the interface was compared with a reference solution without damage. This difficulty does not appear for the Coupling Shell-to-Solid technique, in which the damage included at the local level will affect the global evolution. In this later case, the numerical results would be acceptable while the damage zone was not affected by the coupling between the local and the global level, i.e, the damage zone is far enough from the coupling interfaces.

From the computational standpoint, the Submodeling option needs 30 load increments and 271 iterations to reach a load of 225 kN, whereas the Shell-to-Solid Coupling technique needs 64 load increments and 451 iterations for approximately the same load level. This is due to the fact that in the Coupling Shell-to-Solid technique the damage at the skin-stringer joint influences on the solution process of the whole model, whereas the Submodeling option imposes on the local

model stable and fixed boundary condition evolutions. In fact the Submodeling technique reach the total applied load, 300 kN, whereas the Coupling option finished at around 225 kN due to numerical convergence problems in achieving equilibrium solution.

Both techniques predict damage onset at 50 kN. Figure 7 shows the damage variable evolutions for each technique for 80 (at which the first noise was detected in the test) and 150 kN load levels.

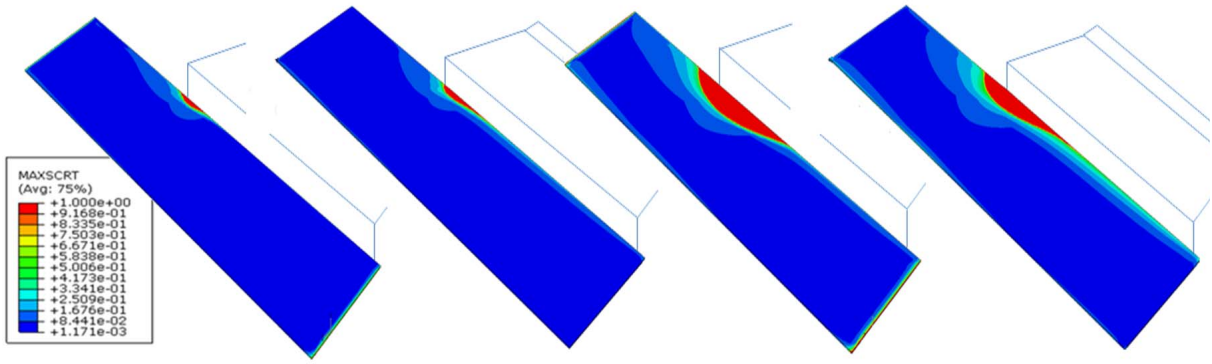

Figure 7. Damage evolution for Submodeling technique: 80 kN (a), 150 kN (c), and Coupling technique: 80 kN (b), 150 kN (d)

Table 2 summarizes the evolution of the damaged zone size with the load for both numerical techniques and their corresponding comparison with the experimental measures. As can be observed, these evolutions seem to be substantially equivalent, leading to the consideration that both options provide similar results in this problem. It is noticeable that, in both cases, the initiation of the failure process at the joint takes place at 50 kN, but the geometric dimensions of the damaged areas were very small (less than 0.5×1 mm^2), being practically undetectable by the experimental measurement devices employed.

Load	Submodeling	Coupling Shel-to-Solid	Experimental test
50 kN	$< 0.5 \times 1$ mm^2	0.5×1 mm^2	Nondetectable
80 kN	2×5 mm^2	2×7 mm^2	Nondetectable
100 kN	4×8 mm^2	4×10 mm^2	$3-4 \times 7-8$ mm^2
150 kN	5×12 mm^2	5×14 mm^2	$5-6 \times 12-15$ mm^2

Table 2. Evolution of the damage zone size

5. Concluding remarks

In the run-out concept analysed, a stable propagation of the damage along the stringer bottom flange at both sides was detected during the loading process. This conclusion was corroborated experimentally and numerically.

The global model was generated using shell element typology, modeling the adhesive layer of the existing joint via continuum elements in order to estimate the stress state and to determine the location and size of the critical regions in the specimen. The local modeling of this zone was

carried out using Submodeling and Shell-to-Solid Coupling techniques. Laminated continuum elements, instead of shell elements, were selected to discretize the desired portions of the skin and the stringer, and using interface cohesive elements for the adhesive layer.

The numerical predictions of the damage onset and propagation path in the specimen at the stringer run-out using both global-local FEM approaches are finally compared with the experimental results. Both techniques produce satisfactory results.

From the numerical point of view, the solution process for the Submodeling technique is robuster than that for the Coupling Shell-to-Solid option. This is due to the fact that the damage considered at the local level affects the solution of the whole model in the Coupling technique. In contrast, the local model is solved separately in the Submodeling case, not affecting the solution of the global one.

References

[1] D.D. Davis Jr., G.L. Farley, D.R. Ambur, R.C. Davis, M.J. Shuart, and Lotts C.G. Wang, J.T. and. An analytically designed subcomponent test to reproduce the failure of a composite wing box beam. In *AIAA Conference Paper, 1993*.

[2] M.J. Shuart, D.R. Ambur, D.D. Davis, R.C. Davis Jr., G.L. Farley, C.G. Lotts, and J.T. Wang. Technical report, NASA Technical Report N9528847, 1992.

[3] B.G. Falzon, G.A.O. Davies, and E. Greenhalgh. Failure of thick-skinned stiffener runout sections loaded in uniaxial compression. *Composite Structures*, 53:223–233, 2001.

[4] B.G. Falzon and D. Hitchings. The behaviour of compressively loaded stiffener runout specimens - part ii: Finite element analysis. *Journal of Composite Materials*, 37(6):481–501, 2003.

[5] B.G. Falzon and G.A.O. Davies. The behaviour of compressively loaded stiffener runout specimens - part i: Experiments. *Journal of Composite Materials*, 37(5):381–400, 2003.

[6] J. Reinoso, A. Blázquez, A. Estefani, F. París, J. Cañas, E. Arévalo, and F. Cruz. Experimental and three-dimensional global-local finite element analysis of a composite component including degradation process at the interfaces. *Composites, Part B*, 43:1929–1942, 2012.

[7] Hibbitt, Karlsson, and Serensen. *ABAQUS/STANDARD. User's Guide and Theoretical Manual. Version 6.8*. 2008.

[8] C.G. Dávila and P.P. Camanho. Analysis of the effects of residual strains and defects on skin/stiffener debonding using decohesion elements. In *SDM Conference, Norfolk, VA, April 7-10, 2003*, 2003.

[9] M.L. Benzeggagh and M. Kenane. Measurement of mixed-mode delamination fracture toughness of unidirectional glass/epoxy composites with mixed-mode bending apparatus. *Composite Science and Technology*, 56(4):439–449, 1996.